Received: 15 November 2021 | Revised: 25 December 2021 | Accepted: 14 January 2022

DOI: 10.1002/bte2.20210017

REVIEW

BATTERY ENERGY Open Access WILEY

Hysteresis in electrochemical systems

Anton Van der Ven[1] | **Kimberly A. See**[2] | **Laurent Pilon**[3]

[1]Materials Department, University of California Santa Barbara, Santa Barbara, California, USA

[2]Division of Chemistry and Chemical Engineering, California Institute of Technology, Pasadena, California, USA

[3]Mechanical and Aerospace Engineering Department, Henry Samueli School of Engineering and Applied Science, University of California Los Angeles, Los Angeles, California, USA

Correspondence
Anton Van der Ven, Materials Department, University of California Santa Barbara, 1361A Engineering II, Santa Barbara, CA 93106-5050, USA.
Email: avdv@ucsb.edu

Funding information
Department of Energy, Basic Energy Sciences, Grant/Award Number: DESC0019381

Abstract

Hysteresis is a phenomenon that pervades both the physical and social sciences. While commonly associated with magnetism, it also occurs in a wide variety of other materials, including ferroelectrics and shape memory alloys. Hysteresis emerges when a particular property has a history dependence. It is exploited in microelectronic memory, logic, and neuromorphic devices. In electrochemical systems, such as Li-ion batteries, hysteresis is undesirable as it leads to energy losses during each round trip charge–discharge cycle. Unfortunately, many new battery concepts that promise significant increases in energy density, including those that rely on displacement and conversion reactions, or on anion-redox mechanisms, suffer from severe hysteresis that prevents their commercialization. This article surveys different forms of hysteresis in electrochemical systems with a focus on Li-ion batteries and establishes thermodynamic and kinetic principles with which to understand and rationalize electrochemical hysteresis. The ability to control hysteresis in rechargeable batteries will enable the implementation of promising electrode chemistries. It will also open the door to many new device applications. As on-chip batteries become more prominent, new possibilities will emerge to incorporate them not only as local energy sources but also as active components of new device concepts that exploit electrochemical hysteresis.

KEYWORDS

batteries and fuel cells, energy, energy efficiency, energy storage, material science

1 | INTRODUCTION

Hysteresis is a well-known phenomenon of ferromagnetic materials, ferroelectrics and shape memory alloys. In hard magnets, the magnetization forms a loop when cycling the external magnetic field.[1] Ferroelectrics can exhibit a similar loop in a polarization versus electric field plot,[2] while shape memory alloys often exhibit a loop in their stress–strain curves.[3] Hysteresis occurs when the response upon increasing an external load (e.g., a magnetic field, electric field or stress) differs from that upon reversing the load, leading to path dependence.

The focus of this overview is to survey hysteresis phenomena in electrochemical cells, and in particular in rechargeable batteries. The intense research on Li-ion batteries over the past three decades has led to a wide variety of battery designs that rely on complex reaction mechanisms within the electrodes, with many of them exhibiting hysteresis in their voltage versus charge curve. Often deemed undesirable when it occurs in batteries,

novel applications[4] that exploit electrochemical hysteresis can also be envisioned. The phenomenon of hysteresis serves as the foundation of many memory,[5,6] logic, and neuromorphic devices.[7,8] Undoubtedly it will play an important role in future quantum devices as well.

Most commercial batteries rely on intercalation processes in which a guest cation, such as Li, fills the interstitial sites of an open host crystal structure.[9,10] The Li storage capacity of intercalation compounds, however, is limited. Other reaction mechanisms that can achieve significantly higher capacities have, therefore, also received much attention. These include alloying reactions,[11] displacement and conversion reactions[12] and reaction mechanisms that rely on alternatives to transition metal redox, such as anion redox processes.[13] It is these more complex reaction mechanisms that lead to novel forms of hysteresis in electrochemical systems that are distinct from the more traditional forms observed in magnetic, ferroelectric, and shape-memory applications.

This overview catalogues different forms of electrochemical hysteresis and describes their mechanisms at a fundamental level in terms of basic thermodynamic and kinetic principles. A distinction is made between dissipative hysteresis due to sluggish kinetic processes, more appropriately called polarization, and other forms of hysteresis that are present even when all kinetic processes are facile. Mechanisms of hysteresis will be illustrated using different Li-ion batteries as examples, but the principles are general and can be applied to many other electrochemical systems.

2 | THERMODYNAMIC PRELIMINARIES

A Li-ion battery consists of a cathode and an anode, separated by an electronically insulating electrolyte that allows the passage of Li^+ ions. The equilibrium voltage of an Li-ion battery, measured in an open circuit, is related to the chemical potentials of Li in the cathode, μ^c_{Li}, and the anode, μ^a_{Li}, according to the Nernst equation[14]

$$V = -\left(\mu^c_{\mathrm{Li}} - \mu^a_{\mathrm{Li}}\right)/e, \tag{1}$$

where e is the elementary charge. In Li-ion batteries that use metallic Li as their anode, μ^a_{Li} is a constant and is equal to that of pure Li. Any variations in the open circuit voltage are then due to variations in μ^c_{Li}, the Li chemical potential of the cathode.

The voltage curve of an actual measurement will deviate from the true equilibrium voltage curve due to polarization and hysteresis. This is because overpotentials are necessary to drive kinetic processes, including electrochemical reactions at the electrode/electrolyte interfaces, cation transport, and the migration of interfaces during phase transformations. In exploring hysteresis phenomena, it will be assumed that the kinetic processes within the anode and electrolyte and those at the electrode/electrolyte interfaces are so facile that their contributions to polarization are negligible. It will also be assumed that the electronic conductivity of the cathode is sufficiently high that electron transport between the reaction front at the electrode/electrolyte interface and the current collector is not rate-limiting. In this somewhat idealized scenario, the voltage is determined by the Li chemical potential at the surface of the cathode particles in direct contact with the electrolyte.[10,14] The only sources of polarization and hysteresis are then restricted to the cathode. It is these phenomena that will be analyzed here. Hysteresis phenomena that emerge from interactions between different electrode particles are not considered. The reader is referred to other studies that have explored these phenomena.[15–20]

3 | POLARIZATION OF SOLID SOLUTIONS

Any change of state requires an imbalance. Cations will only diffuse if gradients in chemical potential are present, which, in turn, are usually a consequence of gradients in concentration.[14,21] Such gradients cause polarization in the voltage curve between charge and discharge.[10] Figure 1 illustrates this for a simple intercalation compound that forms a solid solution with Li. A solid solution has a sloping voltage profile as schematically illustrated by the black curve in Figure 1A.[21] Consider an electrode particle (yellow) immersed in an electrolyte and in contact with carbon black particles (gray) to facilitate the removal and insertion of electrons (Figure 1B). During charge, electrons are extracted from the electrode particles, inducing a release of Li ions from the electrode surface into the electrolyte. The depletion of Li close to the electrode/electrolyte interface creates a Li concentration gradient through the depth of the particle as schematically illustrated in Figure 1C, which represents the Li concentration along the red dashed line in Figure 1B.

While it is exceedingly difficult to measure the instantaneous concentration profile within an individual electrode particle, it is possible to track the average Li concentration simply by integrating the current of the electrons that have been extracted from the electrode. This average concentration, $\bar{x}$, is denoted by the dashed green line in Figure 1C. The measured voltage is not

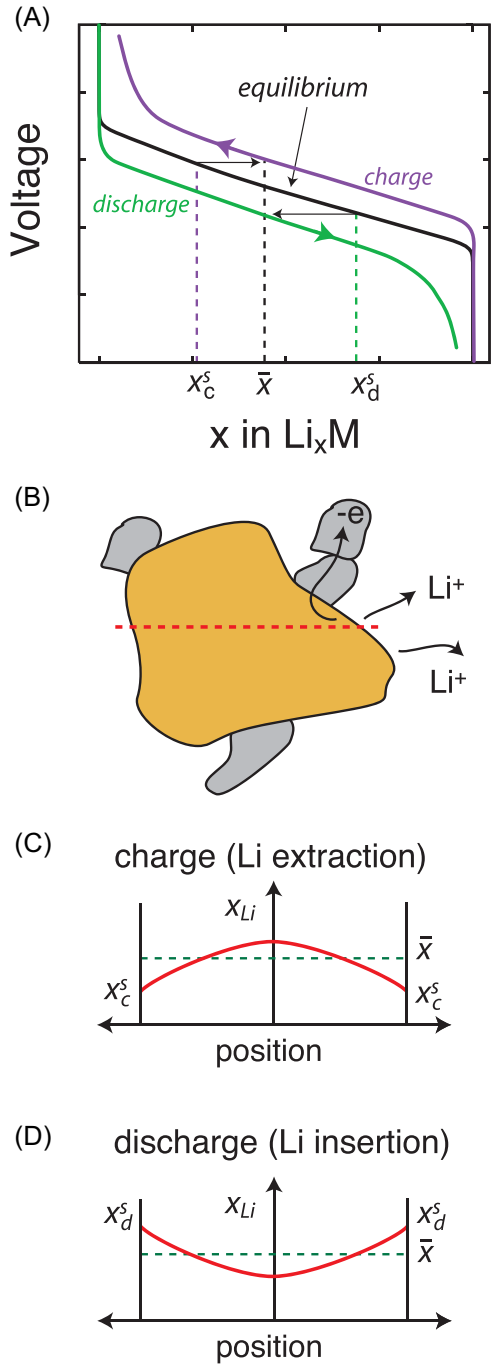

FIGURE 1 Polarization due to Li diffusion in an intercalation compound Li_xM that forms a solid solution with Li. (A) A solid solution exhibits a sloping equilibrium voltage profile (shown in black). Polarization during charge and discharge leads to a charge (discharge) curve that is above (below) the equilibrium voltage curve. (B) Schematic of an electrode particle (yellow) in contact with carbon black (gray) and immersed in an electrolyte. The red dashed line represent a slice along which the Li concentration is plotted during charge in (C) and during discharge in (D)

determined by the average concentration, however, but rather by the concentration at the electrode/electrolyte interface, x_c^s, where the electrochemical reaction takes place.[10] During charging, the Li concentration at the electrode surface, x_c^s, is below that of the average Li concentration, $\bar{x}$, as illustrated in Figure 1C. According to the equilibrium voltage curve of the model solid solution, the voltage at x_c^s is larger than that at $\bar{x}$. Hence, when plotting the measured voltage as a function of the average Li concentration $\bar{x}$ during charging of the electrode, a voltage profile is obtained that is above that of the equilibrium voltage curve. This is schematically illustrated with the purple curve in Figure 1A.

The reverse occurs during discharge (Figure 1D). Li ions are then inserted into the particle at the surface, leading to a local excess in Li close to the surface relative to the average Li concentration $\bar{x}$ (Figure 1D). Since the measured voltage is determined by the concentration at the electrode/electrolyte interface, x_d^s, a plot of the measured voltage versus the average Li concentration, $\bar{x}$, will be lower than the equilibrium voltage curve as schematically illustrated by the green curve in Figure 1A.

The requirement of concentration gradients through the depth of the electrode particles to drive Li diffusion produces a loop in the voltage curve during a full charge (purple) and discharge (green) cycle. The loop is not a true form of hysteresis, but rather a type of polarization. The polarization has a kinetic origin and can be minimized by systematically reducing the rate with which the battery is charged or discharged. In the asymptotic limit of exceedingly slow charge and discharge rates, the measured voltage curve will converge to the true thermodynamic equilibrium curve, and the loop in the voltage versus composition curve essentially disappears. The need for concentration gradients also leads to capacity limitations as described by Radin et al.[10]

4 | HYSTERESIS OF FIRST-ORDER PHASE TRANSITIONS

Hysteresis often accompanies a first-order phase transformation. The principles of phase transformation hysteresis can be illustrated for a simple two-phase reaction in an intercalation compound with the chemical formula Li_xM. This form of hysteresis has many similarities with the hysteresis phenomena of ferromagnets, ferroelectrics, and shape-memory alloys. Figure 2A illustrates an electrode particle undergoing a two-phase reaction during Li insertion, with a Li-rich β phase consuming the original

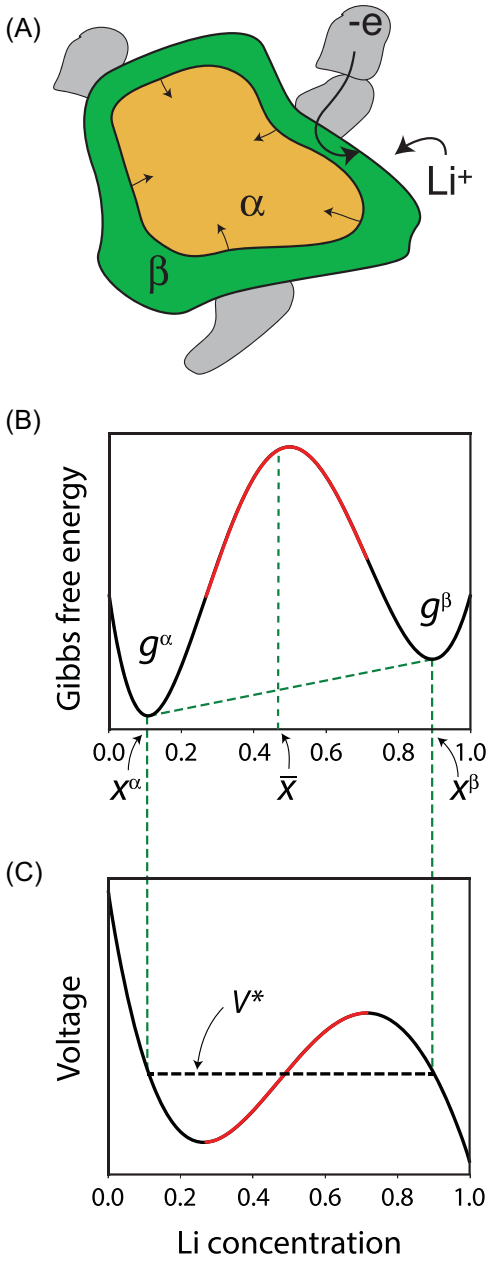

FIGURE 2 (A) A schematic of an electrode particle undergoing a first-order phase transformation through a core-shell mechanism. (B) The simplest free energy curve of an intercalation compound Li_xM that will lead to a first-order phase transformation upon Li insertion or removal. The wells shown in black represent minima corresponding to different phases α and β, while the red region represents an unstable portion where the curvature of the free energy is negative. The free energy of a two-phase mixture (in the absence of coherency strains) resides on the common tangent (dashed line) to the free energy between x^α and x^β. (C) The voltage curve for an intercalation compound with the free energy of (B). The solid line represents the voltage of a solid solution, but the true equilibrium voltage curve follows the plateau at V^* due to the common tangent in (B)

α phase by means of a core-shell growth mechanism. The simplest Gibbs free energy curve that will give rise to such a phase transformation has two wells as a function of the Li concentration, x, as illustrated in Figure 2B. One well corresponds to the α phase, while the other to the β phase. At intermediate concentrations, such as $\bar{x}$, the solid solution is unstable and the compound is prone to decomposing into a two-phase mixture that has a free energy residing on the common tangent shown as the dashed line in Figure 2B. The coexisting phases have compositions x^α and x^β.

The equilibrium voltage curve of an intercalation compound, Li_xM, as measured relative to a metallic Li reference anode, is determined by the shape of the free energy of the compound. This is a consequence of the Nernst equation, Equation (1), which relates the voltage to the Li chemical potential, μ_{Li}^c, of the cathode. The Li chemical potential in turn is linearly related to the slope of the free energy g with respect to x.[14] The voltage for a homogeneous phase having the free energy of Figure 2B is illustrated as the solid line in Figure 2C. It has a nonmonotonic shape due to the unstable region (shown in red) where the Gibbs free energy has a negative curvature. The true equilibrium voltage curve does not have this shape, however, and instead exhibits a plateau between x^α and x^β as shown by the dashed line in Figure 2B. The plateau at V^* emerges due to the two-phase coexistence between x^α and x^β, where the chemical potential, and therefore the voltage, is a constant along the common tangent.

The first-order phase transformation between α and β can also be analyzed with the help of the grand canonical free energy, defined as $\phi = g - x\mu_{Li}$. This is the characteristic thermodynamic potential at constant μ_{Li} (as opposed to constant Li concentration x). Due to the Nernst equation, it is possible to control the Li chemical potential, μ_{Li}, in thermodynamic equilibrium by imposing a particular voltage on the cell through the external circuit. Figure 3A plots the grand canonical free energy, ϕ, as a function of the voltage for the free energy model of Figure 2. Figure 3B shows the same relation between voltage and concentration x of Figure 2C but now with the x and voltage axes interchanged so as to make the voltage the independent axis. Each branch in Figure 3A with a negative curvature corresponds to a local well of the free energy curve g of Figure 2B. The branch corresponding to ϕ^α crosses that of ϕ^β at V^*, the voltage corresponding to the equilibrium plateau voltage.

A first-order phase transformation never occurs precisely at the equilibrium voltage plateau, V^*, but instead requires an overpotential, ΔV, to create a thermodynamic driving force, $\Delta\phi$, to spur the phase change. Figure 3 shows the relationship between an overpotential, ΔV and

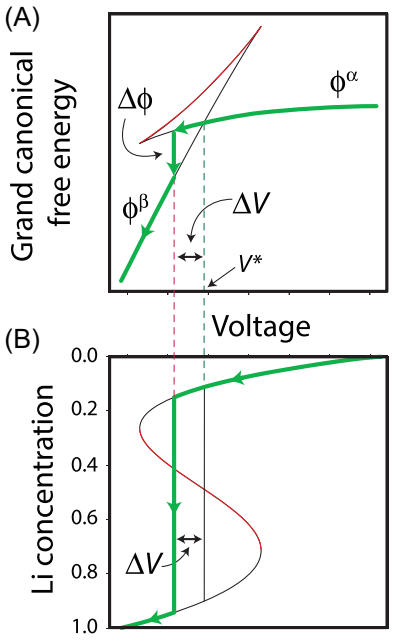

FIGURE 3 A first-order phase transformation can be analyzed in terms of the grand canonical free energy, $\phi = g - x\mu_{Li}$ when controlling the voltage. (A) The grand canonical free energy for the free energy model of Figure 2B. The red portion corresponds to the unstable portion of the free energy in Figure 2B. The green line denotes a possible path when decreasing the voltage starting from the dilute α phase. An overpotential ΔV is always necessary to create a thermodynamic driving force $\Delta\phi$ to overcome phase transformation barriers. (B) The need for a driving force $\Delta\phi$ leads to a polarization of the plateau in the voltage curve that is equal to the overpotential ΔV

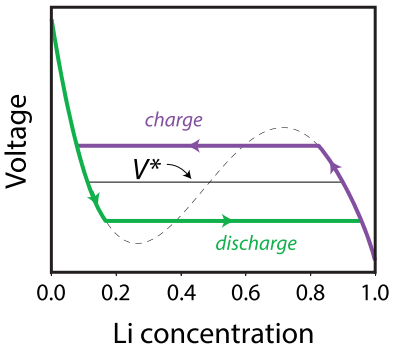

FIGURE 4 Hysteresis in the voltage curve of an intercalation compound undergoing a first-order phase transformation

a thermodynamic driving force when transforming from α to β. At high voltages, the cathode is stable in the dilute α phase. The α phase follows the ϕ^{α} branch in the direction of the green arrow upon decreasing the voltage. Once the voltage reaches V^*, the grand canonical free energies of α and β become equal and a transition from α to β is thermodynamically possible. The transformation will not occur spontaneously, however, until the voltage

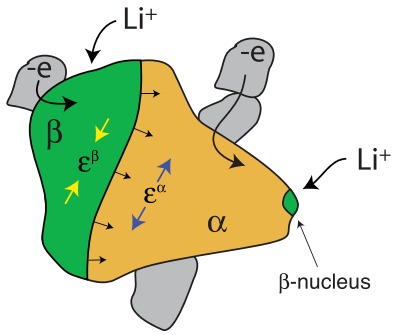

FIGURE 5 A schematic illustrating the different mechanisms that consume the chemical free energy driving force during a first-order phase transformation within an electrode particle. The creation of new interfaces during a nucleation event and the strain energy penalty that accompanies a coherent two-phase coexistence between phases α and β consume a portion of the chemical free energy driving force that is set up by an overpotential. The migration of the interface separating α and β also dissipates free energy as a frictional process. ϵ^{α} and ϵ^{β} represent strains within the α and β phases to enable a coherent two-phase coexistence between the two phases

is decreased below V^* to build up a sufficiently large thermodynamic driving force $\Delta\phi$ that can overcome both dissipative kinetic processes and free energy barriers accompanying the transient two-phase coexistence illustrated in Figure 2A. A similar overpotential ΔV, but in the opposite direction is necessary during charging to induce the reverse transformation from β to α. The result is a hysteresis loop in the voltage curve as illustrated in Figure 4.

There are several ways that an electrode material undergoing a first-order phase transformation can dissipate the thermodynamic driving force $\Delta\phi$ (Figure 5). A first-order phase transformation generally requires a nucleation event, whereby a nano-scale embryo of critical dimensions forms as a result of thermal fluctuations. An interface must be created separating the embryo of the new phase from the original phase. The new interfaces constitute a free energy cost that will consume part of the chemical driving force $\Delta\phi$.[22] Free energy is often also consumed to overcome strain energy penalties that emerge during coherent two-phase coexistence. Most topotactic first-order phase transformations involve phases that have the same host crystal structure but have slightly different lattice parameters. The common host crystal structure allows the phase transformation to proceed as a coherent mixture within the same electrode particle. An electrochemical overpotential is then necessary to build up a chemical free energy driving force to overcome the strain energy cost of coherent two-phase coexistence. Calculations of the coherency strain energy of two-phase coexistence are complex,[23] often requiring a

numerical treatment, but there are several idealized examples that can be solved analytically and that provide insights into the effect of coherency strains on electrochemical properties.[24–26] Finally, a portion of the driving force of a first-order phase transformation, $\Delta\phi$, will be dissipated by the migration of the interface separating the growing phase from the original phase.[27,28]

In contrast to interfacial free energies and coherency strain energies, which temporarily store the free energy driving force, interface migration is similar to diffusion in that it dissipates a free energy driving force as a frictional process.[27,28] As a result, the polarization due to interface migration can be minimized by reducing the charge and discharge rate. This is usually not the case with coherency strain energy penalties, which constitute a thermodynamic barrier[24] that is less sensitive to charge and discharge rates. The overpotentials required to overcome coherency strain energy penalties, therefore, produce a more robust polarization in the voltage curve during a first-order phase transformation that can be viewed as a true form of hysteresis.

While the analysis of phase-transformation hysteresis was illustrated for a topotactic two-phase reaction, similar principles apply to more complex first-order phase transformations.[29] Many intercalation compounds have a layered structure and undergo first-order phase transformations that lead to a change in the stacking sequence of their two-dimensional building blocks, in addition to a change in Li concentration.[10,30,31] This occurs in Li_xCoO_2 at high states of charge[10,32–34] and is especially common in Na- and K-layered intercalation compounds.[30,35–42] Changes in stacking sequence can be mediated through the passage of partial dislocations,[38,43] thereby triggering chemo-mechanical mechanisms of free energy dissipation that are similar to those of plastic deformation in metals. The underlying symmetry of many layered crystal structures also allows for a multiplicity of glide directions that introduce additional irreversibilities responsible for a phenomenon termed electrochemical creep.[44] The result is an accumulation of surface roughening and an overall increase in extended defect formation that consumes additional chemical energy that must be supplied by electrochemical overpotentials.

5 | REACTION PATH HYSTERESIS

The hysteresis phenomena discussed so far arise from the requirement of an overpotential to overcome a barrier. The barrier may either be a sluggish kinetic (i.e., frictional) process that dissipates the electrochemical work required to achieve the overpotential or a high energy intermediate state. Another form of hysteresis that is unique to electrochemical systems occurs when several kinetic processes must be activated during a charge and discharge cycle. Multiple pathways connecting the end states of a lithiation reaction then open up and the path followed during discharge may differ from that followed on the charge, leading to reaction path hysteresis.[45,46] The likelihood of reaction path hysteresis increases with the complexity of the lithiation reaction and with the number of mobile species within the electrode. The following sections describe important classes of electrode materials that exhibit path hysteresis.

5.1 | Displacement and conversion reactions

Very high capacities can be achieved by exploiting Li insertion mechanisms that displace a redox-active transition metal from a host and reduce the displaced cation to the metallic state.[12,47,48] When the reaction occurs topotactically (reconstructively) it is referred to as a displacement (conversion) reaction. Most displacement and conversion reactions are plagued by a substantial degree of hysteresis in their voltage profile. The difference in voltage between charge and discharge can easily exceed 1 Volt.[12] Hysteresis during these reactions often emerges because the path followed during discharge differs from that of charge.

The mechanisms of displacement and conversion reactions have been established in studies of a wide variety of compounds, with notable examples, including Fe and Cu fluorides as potential cathodes[45,49–55] and Cu_2Sb as a candidate anode.[56,57] Fundamental insights about the factors that lead to path hysteresis have been distilled from studies of model electrode chemistries, such as FeF_2[45] and spinel $CuTi_2S_4$.[46,58]

The reaction of Li with $Cu_{0.5}TiS_2$, which undergoes the $Li + Cu_{0.5}TiS_2 \longrightarrow LiTiS_2 + 1/2Cu$ displacement reaction, results in a large hysteresis loop in the voltage profile due to a difference in the kinetic path followed during charge and discharge.[58] The paths can be mapped in a ternary composition space spanned by Li, Cu, and TiS_2 as shown in Figure 6A. The spinel TiS_2 host retains its structure during the reaction as Li insertion leads to the displacement of Cu. Superposed on the ternary composition diagram is a calculated phase diagram at room temperature.[46] Stable compounds include $Cu_{0.5}TiS_2$, $LiTiS_2$, and TiS_2, all three having the same TiS_2 spinel host structure. Both Li and Cu fill interstitial sites of the TiS_2 host as a solid solution but have a limited solubility when both Li and Cu are present as shown

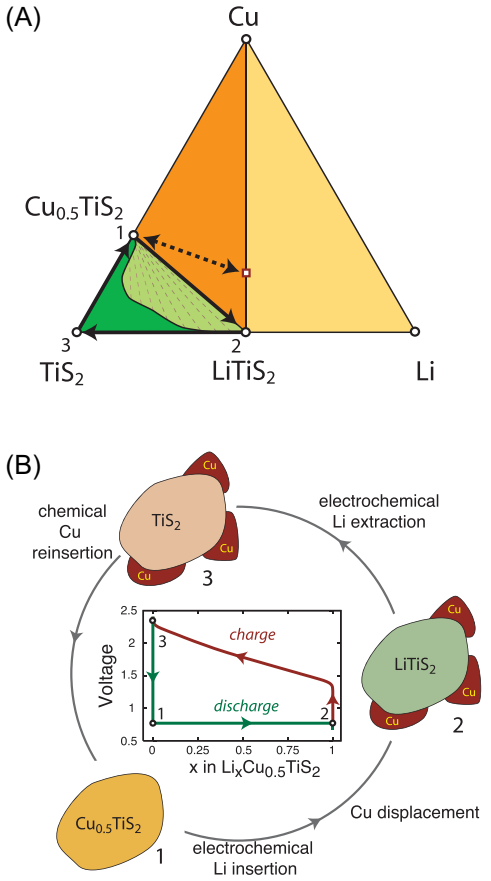

FIGURE 6 The electrochemical insertion of Li into spinel $Cu_{0.5}TiS_2$ results in the formation of $LiTiS_2$ and a displacement of Cu from the spinel host. It is an ideal model system with which to understand the mechanisms of path hysteresis during displacement and conversion reactions. (A) The path followed during discharge and charge can be mapped out in a ternary phase diagram. (B) Due to a large difference in the Li and Cu mobilities within the spinel TiS_2 host, the path followed on discharge differs from that on charge leading to a large hysteresis loop in the voltage curve. Adapted from Reference [46]

by the dark green domain in Figure 6A. When the concentrations of Li and Cu are simultaneously high, a miscibility gap opens up as shown by the two-phase region in light green spanned by the dashed tie lines in Figure 6A.

The overall composition of the electrode during Li insertion into $Cu_{0.5}TiS_2$ upon discharge follows the dashed black line that starts at $Cu_{0.5}TiS_2$ and points toward the Li corner in Figure 6A. The electrode passes through a three-phase region consisting of $Cu_{0.5}TiS_2$, $LiTiS_2$ and metallic Cu (orange triangle). As the Li concentration increases, the fraction of $LiTiS_2$ and metallic Cu increases at the expense of $Cu_{0.5}TiS_2$. Since the TiS_2 hosts of $LiTiS_2$ and $Cu_{0.5}TiS_2$ are the same, the Li insertion process can proceed as a two-phase reaction within the original electrode particle (path 1 to 2) with the third phase Cu precipitating out on the surface of the electrode particles, as schematically illustrated in Figure 6B. At the end of discharge, in state 2, the original $Cu_{0.5}TiS_2$ has completely converted to $LiTiS_2$ and all the Cu has been displaced to the surface. The voltage profile of this reaction is a plateau (Figure 6B) since the Li chemical potential in a three-phase region in a ternary composition space remains constant with composition.

To return to the original state on charge (state 1), Li removal must be accompanied by the reinsertion of Cu into the TiS_2 host. In contrast to the discharge reaction, however, Li extraction and Cu reinsertion can proceed along one of a multitude of pathways. The path that it chooses is sensitive to the relative mobilities of Li and Cu within the TiS_2 spinel host as well as the rate of charge.[46] A first-principles study of diffusion in this system predicted eight orders of magnitude difference in the diffusion coefficients of Li and Cu, with Li being substantially more mobile than Cu in spinel TiS_2.[46] The electrochemical removal of Li is, therefore, very facile and can proceed to completion at typical charging rates before Cu ever has a chance to diffuse into the TiS_2 crystal.

In the most extreme scenario, where Li extraction occurs rapidly compared to time scales required for appreciable Cu diffusion, the charge reaction will follow the path connecting points 2 and 3 in Figure 6A, representing the electrochemical extraction of Li without any Cu reinsertion. It is only after Li has been completely removed that Cu then has a chance to reinsert. The Cu reinsertion into TiS_2, however, occurs chemically, as opposed to electrochemically, since it is decoupled from the electrochemical Li extraction process. The chemical insertion of Cu into TiS_2 comes to completion when the original $Cu_{0.5}TiS_2$ is reformed (from state 3 to state 1). The open circuit voltage curve along this path differs substantially from that during discharge as is clear in Figure 6B, which shows the calculated voltage along the pathway 1 to 2 and 2 to 3. The calculated hysteresis loop is similar to that measured experimentally.[58] It should be noted that the slow extraction of Li during charge, at rates comparable to those of Cu diffusion, may be accompanied by simultaneous reinsertion of Cu, leading to a more curved path in composition space in Figure 6A.

Experimental studies of the displacement reaction of $Cu_{0.5}TiS_2$ using in-situ X-ray diffraction have shown clear evidence that a different path is followed in the ternary composition space spanned by TiS_2, Cu, and Li during charge and discharge.[58] Phase-field simulations relying on first-principles thermodynamic and kinetic data predict similar behavior.[46] These fundamental studies of the $Cu_{0.5}TiS_2$ model system have shown that path hysteresis emerges when multiple cation species are

mobile, with the susceptibility to hysteresis increasing as the difference in mobility between Li and the other mobile species increases.[46] Other more subtle thermodynamic factors also play a role as the extraction of Li must set up sufficiently large driving forces for the reinsertion of displaced transition metals, which is a property of the free energy surface of the compound.[46,57]

5.2 | Li-excess materials and disordered rocksalts

Li-excess materials have received much attention during the past decade due to their ability to deliver high capacities by means of nontraditional redox mechanisms.[59–61] While highly promising, they, unfortunately, suffer from voltage hysteresis.[61–63] Although the redox mechanisms responsible for the anomalous capacity of Li-excess materials remain poorly characterized and understood, they appear to be tied to the presence of oxygen ions that are undercoordinated by transition metal cations.[13,62,64–71] Li-excess materials can be synthesized as having either a layered or a disordered rocksalt crystal structure.[59,60,62,63,72] The various redox mechanisms that have been proposed to explain the anomalous capacity either facilitate[73,74] or require[69,70] transition metal migration, possibly coupled with the detachment of oxygen ions from the crystal to form trapped O_2^{n-} molecular species.[69,70,75]

Figure 7 shows[76] the voltage profile of a typical Li-excess compound having a layered crystal structure that is made of a coherent mixture of $Li(Ni_{1-y-z}Mn_yCo_z)O_2$ (NMC) and Li_2MnO_3.[62,63] The Li_2MnO_3 component is Li-excess in the sense that its Li to Mn ratio is greater than one. The initial sloping region on the first charge is due to the NMC component, which ends when all transition metals have reached an oxidation state of +4. This is followed by an activation plateau, where excess capacity is extracted. The voltage profile on discharge has a different shape from that of the first charge, strongly suggesting that the electrode material has undergone structural changes. The first charge voltage profile is never recovered on subsequent cycles and a hysteresis loop persists. Furthermore, the shapes of the charge and discharge voltage profiles evolve over time and the average voltage gradually decreases with each cycle, a phenomenon referred to as voltage fade.

While the structural changes that occur during the activation plateau and during subsequent cycling remain to be precisely characterized experimentally, it is now well established that transition metal ions migrate and that trapped O_2^{n-} molecular species may form and cleave during Li insertion and removal.[61–63] The occurrence of

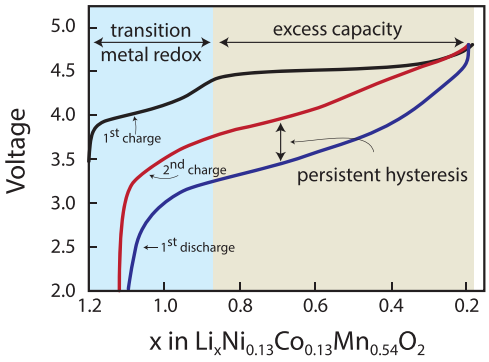

FIGURE 7 Li-excess materials consisting of a coherent mixture of layered NMC ($Li(Ni_{1-y-z}Mn_yCo_z)O_2$) and Li_2MnO_3 exhibit an anomalous capacity that cannot be explained by traditional transition metal redox mechanisms. The first charge is accompanied by an activation step, characterized by a voltage plateau around 4.5V. Subsequent cycles are characterized by persistent hysteresis. Adapted from Reference [76]

cation and anion migration within the crystal during electrochemical Li insertion and extraction makes the electrode susceptible to path hysteresis in a way that is similar to that exhibited by displacement and conversion reactions as described in the previous section. The parallel with displacement and conversion reactions becomes apparent upon the introduction of order parameters[77,78] that track the degree of disorder among transition metals and/or the extent with which O_2^{n-} molecular species have formed. For example, when the transition metal cations occupy either octahedral or tetrahedral sites depending on their oxidation state,[69] a suitable order parameter, η, would track the fraction of filled tetrahedral sites. Alternatively, if redox processes occur through the formation and cleavage of trapped O_2^{n-} molecular species during charge and discharge, then the order parameter would track the number of O_2^{n-} molecular species. More sophisticated order parameters can be devised[77] when tracking the degree of long-range order among transition metals in the host.

The free energy of the electrode material is a function not only of the Li concentration but also of any relevant order parameters.[77,78] Figure 8A illustrates a free energy surface as a function of Li concentration and a simple order parameter, η, for a hypothetical intercalation compound (e.g., a disordered rocksalt) in which cations or anions are mobile. The equilibrium state of the electrode at a fixed Li concentration is determined by the minimum in the free energy with respect to the order parameter η. In this hypothetical example, the minimum in the free energy of Figure 8A with respect to the order parameter shifts with Li concentration.

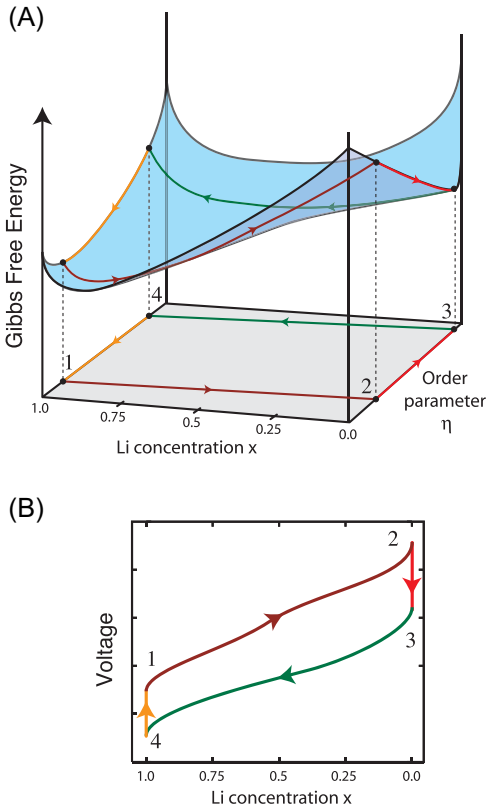

FIGURE 8 Path hysteresis can occur in electrodes that contain mobile transition metals or anions. The state of the cation and/or anion ordering within the electrode material can be tracked with order parameters, η. (A) The free energy of the electrode material will not only be a function of the Li concentration but also of the order parameter. Path hysteresis can occur if the Li mobility is higher than that of the transition metals/anions, whereby a different portion of the free energy surface is traversed during discharge as compared with the charge. The result is a hysteresis loop in the voltage profile (B)

A free energy surface as that of Figure 8A makes the electrode material susceptible to path hysteresis when the mobilities of the cations or anions tracked by the order parameter are more sluggish than that of Li. For example, rapid charging will lead to Li extraction at fixed order parameter, denoted by path 1 to 2 in Figure 8A. At high states of charge ($x = 0$), a strong driving force sets in for the cations to reorder and attain the minimum free energy at a finite value of the order parameter in state 3. This change of state, which occurs at a constant Li concentration, is a chemical reordering process, without any exchange of electrochemical work. On discharge, a different path is therefore followed, whereby Li insertion again occurs at a constant value of the order parameter, taking it to state 4 (Figure 8A). At the end of discharge, the cations will again reorder to reach the minimum free energy at $x = 1$. The voltage curve, when neglecting dissipative kinetic processes, is, according to the Nernst equation (Equation 1), related to the slope of the free energy with respect to Li concentration. Since a different path is followed in composition and order parameter space during charge and discharge, the voltage profile during charge will differ from that during discharge, leading to a hysteresis loop as schematically illustrated in Figure 8B. The degree of hysteresis in the voltage profile will depend on the shape of the free energy surface as a function of the order parameter(s) and the difference in mobility between Li and the mobile cations/anions within the compounds.

It should be emphasized that the true origins of hysteresis in Li-excess and disordered rocksalts remain to be fully established. Many questions persist about the structural changes that occur during each charge and discharge cycle. More precision is needed in the identification of relevant order parameters that track these structural changes. Furthermore, in contrast to many common electrode materials, Li-excess materials and disordered rocksalts tend to be poor electronic conductors.[72] Sluggish electronic conductivity is not only responsible for polarization in the voltage curve, but may also open up additional asymmetries in kinetic pathways between charge and discharge, especially if redox states are localized. It is well-known, for example, that charge ordering phenomena, whereby localized oxidation states order over the transition metal sites, can lead to hysteresis phenomena, even in intercalation compounds, as was elucidated for $Li_3V_2(PO_4)_3$.[79] In this context, order parameters can again be invoked to track the degree of charge ordering, in addition to the order parameters that describe the degree of metal and/or anion disorder. Sluggish electronic transitions between different adiabatic free energy surfaces, with each free energy corresponding to a particular electronic configuration, have also been invoked as a cause of hysteresis in disordered rocksalts.[80]

5.3 | Path hysteresis accompanying sulfur anion redox

Anion redox in oxides yields high capacity at high potentials, but the many side reactions that can occur at these high potentials convolute mechanistic studies. Various spectroscopies are used to probe charge compensation mechanisms but if the electrolyte is decomposing in addition to the oxidation of the material, it can be difficult to determine the origin of spectroscopic features. Sulfide oxidation, on the other hand, occurs at lower potentials due to the higher energy S p states and thus sulfides provide an opportunity to study anion redox within the voltage window of electrolytes. Additionally,

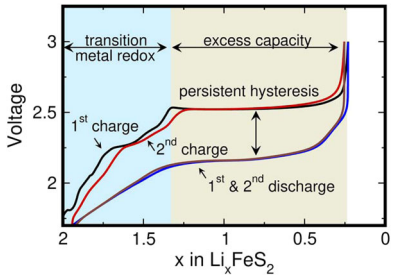

FIGURE 9 The Li-excess sulfide Li_2FeS_2 is capable of reversible multielectron redox. The initial sloping region in the charge curve corresponds to Fe oxidation and the subsequent plateau corresponds to sulfide oxidation. The discharge curve reveals path hysteresis, but the reduced product is very similar to the pristine material resulting in a nearly identical charge curve on cycle 2. Adapted from Reference [82]

Li-excess sulfides can be prepared with abundant metals, like Fe, compared to the less abundant metals used in oxides, like Ni and Co.

The Li-excess metal sulfide Li_2FeS_2 is discussed first as a case study. Different from the Li-excess oxides, the Li_2FeS_2 structure is characterized by hexagonally closed-packed layers of sulfur and alternating layers of edge-sharing octahedral Li with edge-sharing tetrahedral mixed site Fe/Li (50/50).[81] Figure 9 shows the discharge and charge curves of the first and second cycles of Li_2FeS_2. The charge curve is characterized first by a sloping region below 2.5 V, followed by a long plateau. The primary charge compensation mechanism in the sloping region is the oxidation of Fe^{2+} to mixed $Fe^{2+/3+}$, which accounts for approximately 0.5 electrons per formula unit (f.u.).[82] Above 2.5 V, S^{2-} is oxidized to $(S_2)^{2-}$ accounting for almost one electron per f.u.[82] The subsequent discharge curve is shifted negative by approximately 0.36 V. The shape of the discharge curve reflects that of the charge curve to some degree, although the features are smeared out and the kinks observed at lower potentials are not observed. Importantly, the hysteresis and shape differences cannot be attributed to kinetic effects.[82] The presence of the hysteresis and the changes in shape suggests that the reduction path does not mirror the oxidation path. In the oxides, such path hysteresis is attributed in part to metal migration. Here, however, Fe remains tetrahedral throughout the charge,[82] which suggests that it is not migrating to the now vacant octahedral sites, although it could be migrating among the tetrahedral sites. The path hysteresis is additionally observed in the asymmetric evolution of the (001) reflection upon charge and discharge.[82] If the material is cycled below 2.5 V, the hysteresis is largely absent. Thus, the hysteresis originates from the structural changes incurred during anion oxidation.

A notable difference between the sulfides and oxides is observed on cycle 2. In Li_2FeS_2, the shape of the charge curve on cycle 2 is nearly identical to that measured on cycle 1 (Figure 9). Therefore, while Li_2FeS_2 exhibits path hysteresis during each charge/discharge cycle, the discharged material returns to its original crystallographic state, being structurally very similar to the pristine material even though a different path is traveled upon reduction. Such a result suggests that the sulfide/persulfide structural distortion is reversible. Persistent and reproducible path hysteresis from cycle 1 to cycle 2 has also been observed in the Li-S system, which undergoes significant conversion reactions involving extensive S-S bond breaking and forming although through very different mechanisms.[83]

Interestingly, the reproducibility of the cycle 1 hysteresis in cycle 2 is not universal to Li-excess sulfides. For instance, the charge curve of Fe substituted $Li_2(Sn/Ti)S_3$ (i.e., $Li_{1.33-2y/3}(Sn/Ti)_{0.67-y/3}Fe_yS_2$) is significantly different from cycle 1 to cycle 2, more similar to the electrochemistry of the oxides.[84,85] The first cycle exhibits path hysteresis, similar to Li_2FeS_2, and metal migration is similarly ruled out. Interestingly, when $Li_{1.13}Ti_{0.57}Fe_{0.3}S_2$ is cycled, the hysteresis slowly fades.[84]

6 | HEAT DISSIPATION DUE TO HYSTERESIS

Polarization and hysteresis lead to the dissipation of useful electrochemical work. The energy lost during a round-trip charge–discharge cycle is equal to the area enclosed by the hysteresis loop. This electrochemical work is ultimately dissipated as heat. Indeed, the change in internal energy, ΔU, of the battery after a full charge/discharge cycle is equal to zero since the battery has returned to its original state (assuming that the effects of mechanical damage or irreversible side reactions can be neglected). According to the first law of thermodynamics, $\Delta U = W + Q$, where W is the net work performed on the battery and Q is the heat transferred from the environment to the battery. The convention is adopted that W and Q are positive when work and heat are supplied to the battery. The net work W performed on a battery during a round-trip cycle is always positive due to polarization and hysteresis. Thus, over a cycle where $\Delta U = 0$ it follows that $Q = -W$. The electrochemical losses W are therefore completely converted to heat released to the environment. The wider the hysteresis loop in the charge/discharge voltage profile, the larger the amount of electrochemical work dissipated as heat. The next two sections describe mechanisms of heat dissipation due to polarization and path hysteresis.

6.1 | Heat dissipation due to polarization

Polarization due to sluggish kinetics within the cathode dissipates heat through frictional processes, such as diffusion and interface migration. Overpotentials that are necessary to overcome the strain energy that is built up during a transient two-phase coexistence is generally also dissipated as heat, in a manner similar to that of shape memory alloys.[3]

There are at least two ways that transporting ions dissipate heat. In electrodes that are semiconductors or insulators, electric fields can emerge within the electrode particles. The transport of ions in an electric field results in a form of Joule heating.[86] Even in the absence of internal electric fields, as in metallic electrode materials, ion diffusion can lead to heat evolution due to changes in the enthalpy of the electrode. Concentration gradients throughout the electrode particle are accompanied by a nonuniform variation of the local enthalpy. As the Li ions diffuse and thereby flatten concentration gradients, the overall enthalpy of the electrode material changes as well, leading to the release of heat if the enthalpy of mixing of the intercalation compound is negative. This form of heat production is referred to as the heat of mixing due to diffusion.[87,88] Electron transport within the electrode will also contribute resistive losses when the electronic conductivity is low. Other kinetic processes such as interface migration during a first-order phase transition also lead to heat production.

While the focus of this overview is on polarization and hysteresis phenomena in the cathode, heat is generated throughout the battery as a result of the electrochemical reactions at the electrode/electrolyte interfaces and ion transport through the electrolyte.[86,89] In battery materials, heat dissipation due to Joule heating dominates while the contribution from the enthalpy of mixing becomes significant at high charging rates when concentration gradients are the largest.[90–92]

6.2 | Heat dissipation due to path hysteresis

Additional mechanisms of heat dissipation occur during path hysteresis that are qualitatively different from those described in the previous section for simple intercalation reactions. Path hysteresis can occur with minimal polarization but still produce a sizable loop in the voltage profile. The voltage curve shown in Figure 6B for the $Li+Cu_{0.5}TiS_2$ displacement reaction, for example, was calculated using the equilibrium Li chemical potential along the path mapped out in Figure 6A.[46] It neglects any polarization due to dissipative kinetic processes or overpotentials that are needed to overcome nucleation barriers and coherency strain energy. The separate paths are therefore assumed to be reversible electrochemical processes. Nevertheless, the large hysteresis loop in the voltage profile still results in the dissipation of useful electrochemical work as heat.

The net work w, per number of TiS_2 units, performed during the reversible electrochemical discharge (1⟶2) and charge (2⟶3) paths of the $Li+Cu_{0.5}TiS_2$ displacement reaction of Figure 6, is equal to

$$w = \oint -eV\,dx = \int_1^2 -eV\,dx + \int_2^3 -eV\,dx = \Delta g_{1\longrightarrow 3}, \qquad (2)$$

where e is the elementary charge, V is the voltage, and $\Delta g_{1\longrightarrow 3}$ is the difference in free energy between states 3 and 1 (i.e., $g_{TiS_2} + 1/2g_{Cu} - g_{Cu_{0.5}TiS_2}$). Here as well, the free energies are normalized by the number of TiS_2 units. The second equality relating w to the difference in the free energy $\Delta g_{1\longrightarrow 3}$ follows from the Nernst equation for reversible paths, Equation (1), and the relationship between the Li chemical potential and the free energy.[14] No electrochemical work is performed between 3 and 1 as no Li ions are exchanged between the anode and cathode along this portion of the cycle.

It is straightforward to verify that the heat q (per TiS_2 unit) that is evolved to the environment during a full cycle is indeed exactly equal to $-w$. When paths 1 to 2 and 2 to 3 occur reversibly (i.e., without polarization), the heat exchanged with the environment is equal to $T\Delta s_{1\longrightarrow 2}$ and $T\Delta s_{2\longrightarrow 3}$, where s is the entropy (per TiS_2) and T is the temperature, assumed to be constant during cycling. The total heat exchange between states 1 and 3 is then $T\Delta s_{1\longrightarrow 3} = -T\Delta s_{3\longrightarrow 1}$. Heat is also released during the chemical mixing step at the end of charge when Cu irreversibly diffuses back into the TiS_2 host (from state 3 to 1). The heat released during this irreversible mixing process is equal to the enthalpy of mixing, $\Delta h_{3\longrightarrow 1}$ (per TiS_2). The total amount of heat exchanged with the environment during a full cycle is the sum of these terms, $q = \Delta h_{3\longrightarrow 1} - T\Delta s_{3\longrightarrow 1}$, which is also equal to $\Delta g_{3\longrightarrow 1}$, the free energy of mixing to form $Cu_{0.5}TiS_2$ when starting from a two-phase mixture of TiS_2 and 1/2Cu. As required by the first law of thermodynamics for a complete cycle, this is equal to minus the positive work performed on the electrode (i.e., $-w = -\Delta g_{1\longrightarrow 3}$), signifying that $q < 0$, that is, heat is transferred to the environment.

The example of the $Li+Cu_{0.5}TiS_2$ displacement reaction shows that there are at least two ways in which

heat is exchanged between the battery and the environment during a charge/discharge cycle that exhibits path hysteresis, even when the effects of polarization are neglected. The first occurs along the electrochemical paths, which will exchange a net quantity of heat since the electrochemical paths do not return the electrode to its original state. The heat evolved along reversible electrochemical paths is equal to $T\Delta s$, where Δs is the net change in entropy along the electrochemical portions of the cycle. The second form of heat production is due to a change in enthalpy that occurs when the electrode irreversibly relaxes to a lower free energy state. This portion of the cycle is a spontaneous chemical process that is decoupled from the external circuit as it does not involve the transfer of Li ions between the cathode and the anode.

7 | DESIGN PRINCIPLES

Several design principles can be formulated to help mitigate or enhance electrochemical hysteresis. In energy storage applications it is desirable to minimize polarization and hysteresis to reduce round-trip energy losses. Applications, such as memory, logic and neuromorphic devices, in contrast, often leverage hysteresis phenomena that are robust and reproducible.

Polarization in the voltage curves of intercalation compounds can be minimized by making unit kinetic processes, such as diffusion and interface migration more facile. Electrode materials that enable fast Li transport, as manifested by large Li diffusion coefficients, will incur less polarization in the voltage profile than those in which Li transport is sluggish. The guest cation diffusion coefficient of intercalation compounds is very sensitive to the host crystal structure, its chemistry, and the overall guest ion concentration. Variations in lattice parameters with guest ion concentration and the onset of correlated diffusion in the concentrated regime can produce orders of magnitude changes in the guest ion diffusion coefficient.[21,93–98]

Overpotentials of first-order phase transformations can be minimized if the coexisting phases have very similar lattice parameters. This reduces the strain energy of coherent two-phase coexistence that needs to be overcome with an overpotential. Interfacial free energies between coexisting phases also need to be small to suppress the need for large overpotentials to nucleate a new phase.

Several strategies can be pursued to minimize path hysteresis.[22,46,57] The presence of mobile species that are not electrochemically active increases the number of kinetic pathways that can be followed during charge and discharge, making the electrode prone to kinetic asymmetries. In a displacement reaction, for example, only one path is available during discharge, since the insertion of Li into the electrode must often be accompanied by the simultaneous removal of a transition metal cation to vacate sites for Li occupancy. Electrochemical Li extraction, in contrast, can often proceed along a multitude of pathways, as the reinsertion of the displaced metal cations is not essential. This form of asymmetry can be minimized by increasing the diffusion coefficient of the displaced metal cation relative to that of Li.[46] The free energy of the compound can also be engineered in a way to ensure that a small overpotential in the Li chemical potential produces a large driving force for the reinsertion of the displaced metal cation.[57] The two factors together then increase the likelihood that the discharge path is retraced during charge.

When metal cations are mobile within the compound, as in Li-excess materials, kinetic asymmetries emerge due to particular crystallographic features of the host. For example, transition metal migration during Li extraction may be restricted to one hop path (e.g., from an octahedral site to an adjacent tetrahedral site). However, upon the reinsertion of Li, the migrated transition metal cation may have multiple hop options, with only one of the hop paths taking the transition metal back to its original site in the fully lithiated state.[69,99] An asymmetry in the entropy associated with hop paths, therefore, emerges. This scenario can lead to a progressive disordering of the original compound during each cycle. The suppression of this type of path hysteresis can be achieved by alterations to the crystal structure that prevent transition metal migration altogether, or that limit transition metal migration to the same pair of sites. The first strategy has been successfully realized in Li-excess-like compounds, such as layered $Na_2Mn_3O_7$,[100,101] where the presence of Na as opposed to Li increases the spacing between Mn_3O_7 layers and thereby suppresses Mn migration.[102]

Many battery concepts that promise very high capacities, such as Li-air and Li-sulfur batteries, suffer from sizable voltage hysteresis that has prevented their widespread commercialization.[103–105] While still poorly understood, hysteresis in these systems can also be attributed to asymmetries in kinetic paths between charge and discharge due to a multitude of possible reaction mechanisms. However, compared to the examples described in this overview, additional considerations arise as the kinetic processes of Li-air and Li-sulfur batteries are highly coupled to processes within the electrolyte and at the electrode/electrolyte interface.[83,104] Furthermore, the reaction products of Li-air and Li-sulfur batteries are electronic insulators, which can lead to additional kinetic asymmetries between charge and discharge.[103,105] Fully understanding voltage hysteresis in Li-air and Li-sulfur batteries will

require identification of all relevant reaction coordinates and order parameters and careful mapping of the relevant free energy surfaces in this variable space.

8 | CONCLUSION

Electrochemical hysteresis comes in many forms. The focus of this overview has been on the hysteresis phenomena in electrode materials of rechargeable batteries. Electrodes consisting of simple intercalation compounds are susceptible to the classical forms of hysteresis that are well understood in magnetic and ferroelectric materials. New forms of hysteresis emerge in electrochemical systems when two or more chemical species are mobile, thereby opening up a multitude of kinetic pathways that introduce asymmetries between charge and discharge. This can lead to path hysteresis, which plagues displacement and conversion reactions as well as the Li-excess and disordered rocksalt materials that achieve high capacities by nonconventional redox processes. The distinct forms of hysteresis can be understood in terms of basic thermodynamic and kinetic principles. This understanding is crucial to enable the design of electrode reaction mechanisms with a prescribed degree of hysteresis. While undesirable for battery applications, the ability to control hysteresis electrochemically opens up many new opportunities in other fields where hysteretic behavior can be exploited in device applications.

ACKNOWLEDGMENTS

This study was supported as part of the Center for Synthetic Control Across Length-scales for Advancing Rechargeables (SCALAR), an Energy Frontier Research Center funded by the U.S. Department of Energy, Office of Science, Basic Energy Sciences under Award # DE-SC0019381.

CONFLICT OF INTERESTS

The authors declare that there are no conflict of interests.

DATA AVAILABILITY STATEMENT

The data presented in this study are available on request from the corresponding author.

ORCID

Anton Van der Ven http://orcid.org/0000-0002-2679-8909

ENDNOTE

[1] This is true in the assumption that there are no other sluggish kinetic processes in the battery outside the cathode that cause additional polarization.

REFERENCES

1. Bertotti G. *Hysteresis in Magnetism: For Physicists, Materials Scientists, and Engineers*. Gulf Professional Publishing; 1998.
2. Damjanovic D. Ferroelectric, dielectric and piezoelectric properties of ferroelectric thin films and ceramics. *Rep Prog Phys*. 1998;61(9):1267.
3. Wollants P, Roos JR, Delaey L. Thermally-and stress-induced thermoelastic martensitic transformations in the reference frame of equilibrium thermodynamics. *Progr Mater Sci*. 1993;37(3):227-288.
4. Li Y, Chueh WC. Electrochemical and chemical insertion for energy transformation and switching. *Ann Rev Mater Res*. 2018;48:137-165.
5. Bhatti S, Sbiaa R, Hirohata A, Ohno H, Fukami S, Piramanayagam S. Spintronics based random access memory: a review. *Mater Today*. 2017;20(9):530-548.
6. Schenk T, Mueller S. A new generation of memory devices enabled by ferroelectric hafnia and zirconia. In: *2021 IEEE 863 International Symposium on Applications of Ferroelectrics (ISAF)*. IEEE; 2021:1-11.
7. Strukov DB, Snider GS, Stewart DR, Williams RS. The missing memristor found. *Nature*. 2008;453(7191):80-83.
8. Yang JJ, Strukov DB, Stewart DR. Memristive devices for computing. *Nat Nanotechnol*. 2013;8(1):13-24.
9. Whittingham MS. Lithium batteries and cathode materials. *Chem Rev*. 2004;104(10):4271-4302.
10. Radin MD, Hy S, Sina M, et al. Narrowing the gap between theoretical and practical capacities in Li-ion layered oxide cathode materials. *Adv Energy Mater*. 2017;7(20):1602888.
11. Obrovac M, Chevrier V. Alloy negative electrodes for Li-ion batteries. *Chem Rev*. 2014;114(23):11444-11502.
12. Cabana J, Monconduit L, Larcher D, Palacin MR. Beyond intercalation-based Li-ion batteries: the state of the art and challenges of electrode materials reacting through conversion reactions. *Adv Mater*. 2010;22(35):E170-E192.
13. Assat G, Tarascon JM. Fundamental understanding and practical challenges of anionic redox activity in Li-ion batteries. *Nat Energy*. 2018;3(5):373-386.
14. Van der Ven A, Deng Z, Banerjee S, Ong SP. Rechargeable alkali-ion battery materials: theory and computation. *Chem Rev*. 2020;120(14):6977-7019.
15. Dreyer W, Jamnik J, Guhlke C, Huth R, Moškon J, Gaberšček M. The thermodynamic origin of hysteresis in insertion batteries. *Nat Mater*. 2010;9(5):448-453.
16. Li Y, ElGabaly F, Ferguson TR, et al. Current-induced transition from particle-by-particle to concurrent intercalation in phase-separating battery electrodes. *Nat Mater*. 2014;13(12):1149-1156.
17. Orvananos B, Malik R, Yu HC, et al. Architecture dependence on the dynamics of nano-$LiFePO_4$ electrodes. *Electrochim Acta*. 2014;137:245-257.
18. Lim J, Li Y, Alsem DH, et al. Origin and hysteresis of lithium compositional spatiodynamics within battery primary particles. *Science*. 2016;353(6299):566-571.
19. Li Y, Chen H, Lim K, et al. Fluid-enhanced surface diffusion controls intraparticle phase transformations. *Nat Mater*. 2018;17(10):915-922.

20. Zhang W, Yu HC, Wu L, et al. Localized concentration reversal of lithium during intercalation into nanoparticles. *Sci Adv*. 2018;4(1):eaao2608.
21. Van der Ven A, Bhattacharya J, Belak AA. Understanding Li diffusion in Li-intercalation compounds. *Acc Chem Res*. 2013;46(5):1216-1225.
22. Chang D, Huo H, Johnston KE, et al. Elucidating the origins of phase transformation hysteresis during electrochemical cycling of Li-Sb electrodes. *J Mater Chem A*. 2015;3(37):18928-18943.
23. Rudraraju S, Van der Ven A, Garikipati K. Mechanochemical spinodal decomposition: a phenomenological theory of phase transformations in multi-component, crystalline solids. *NPJ Comput Mater*. 2016;2(1):1-9.
24. Van der Ven A, Garikipati K, Kim S, Wagemaker M. The role of coherency strains on phase stability in Li_xFePO_4: needle crystallites minimize coherency strain and overpotential. *J Electrochem Soc*. 2009;156(11):A949.
25. Cahn JW. Coherent fluctuations and nucleation in isotropic solids. *Acta Metallurgica*. 1962;10(10):907-913.
26. Voorhees PW, Johnson WC. The thermodynamics of elastically stressed crystals. *Solid State Phys Adv Res Appl*. 2004:59:1-201.
27. Langer J, Sekerka R. Theory of departure from local equilibrium at the interface of a two-phase diffusion couple. *Acta Metall*. 1975;23(10):1225-1237.
28. Hillert M. Solute drag, solute trapping and diffusional dissipation of Gibbs energy. *Acta Mater*. 1999;47(18):4481-4505.
29. Yu YS, Kim C, Liu Y, et al. Nonequilibrium pathways during electrochemical phase transformations in single crystals revealed by dynamic chemical imaging at nanoscale resolution. *Adv Energy Mater*. 2015;5(7):1402040.
30. Delmas C, Fouassier C, Hagenmuller P. Structural classification and properties of the layered oxides. *Phys Bs+c*. 1980;99(1-4):81-85.
31. Delmas C, Carlier D, Guignard M. The layered oxides in lithium and sodium-ion batteries: a solid-state chemistry approach. *Adv Energy Mater*. 2021;11(2):2001201.
32. Amatucci G, Tarascon J, Klein L. CoO_2, the end member of the Li_xCoO_2 solid solution. *J Electrochem Soc*. 1996;143(3):1114.
33. Van der Ven A, Aydinol M, Ceder G, Kresse G, Hafner J. First-principles investigation of phase stability in Li_xCoO_2. *Phys Rev B*. 1998;58(6):2975.
34. Chen Z, Lu Z, Dahn J. Staging phase transitions in Li_xCoO_2. *J Electrochem Soc*. 2002;149(12):A1604.
35. Yabuuchi N, Kubota K, Dahbi M, Komaba S. Research development on sodium-ion batteries. *Chem Rev*. 2014;114(23):11636-11682.
36. Radin MD, Van der Ven A. Stability of prismatic and octahedral coordination in layered oxides and sulfides intercalated with alkali and alkaline-earth metals. *Chem Mater*. 2016;28(21):7898-7904.
37. Vinckeviciute J, Radin MD, Van der Ven A. Stacking-sequence changes and Na ordering in layered intercalation materials. *Chem Mater*. 2016;28(23):8640-8650.
38. Kaufman JL, Vinckeviciute J, Kolli SK, Goiri JG, Van der Ven A. Understanding intercalation compounds for sodium-ion batteries and beyond. *Philos Trans Royal Soc A*. 2019;377(2152):20190020.
39. Kaufman JL, Van der Ven A. Na_xCoO_2 phase stability and hierarchical orderings in the O3/P3 structure family. *Phys Rev Mater*. 2019;3(1):015402.
40. Toriyama MY, Kaufman JL, Van der Ven A. Potassium ordering and structural phase stability in layered K_xCoO_2. *ACS Appl Energy Mater*. 2019;2(4):2629-2636.
41. Kaufman JL, Van der Ven A. Ordering and structural transformations in layered K_xCrO_2 for K-ion batteries. *Chem Mater*. 2020;32(15):6392-6400.
42. Hasa I, Mariyappan S, Saurel D, et al. Challenges of today for Na-based batteries of the future: from materials to cell metrics. *J Power Sources*. 2021;482:228872.
43. Gabrisch H, Yazami R, Fultz B. The character of dislocations in $LiCoO_2$. *Electrochem Solid State Lett*. 2002;5(6):A111.
44. Radin MD, Alvarado J, Meng YS, Van der Ven A. Role of crystal symmetry in the reversibility of stacking-sequence changes in layered intercalation electrodes. *Nano Lett*. 2017;17(12):7789-7795.
45. Doe RE, Persson KA, Meng YS, Ceder G. First-principles investigation of the Li-Fe-F phase diagram and equilibrium and nonequilibrium conversion reactions of iron fluorides with lithium. *Chem Mater*. 2008;20(16):5274-5283.
46. Yu HC, Ling C, Bhattacharya J, Thomas JC, Thornton K, Van der Ven A. Designing the next generation high capacity battery electrodes. *Energy Environ Sci*. 2014;7(5):1760-1768.
47. Poizot P, Laruelle S, Grugeon S, Dupont L, Tarascon J. Nano-sized transition-metal oxides as negative-electrode materials for lithium-ion batteries. *Nature*. 2000;407(6803):496-499.
48. Morcrette M, Rozier P, Dupont L, et al. A reversible copper extrusion-insertion electrode for rechargeable Li batteries. *Nat Mater*. 2003;2(11):755-761.
49. Yamakawa N, Jiang M, Key B, Grey CP. Identifying the local structures formed during lithiation of the conversion material, iron fluoride, in a Li ion battery: a solid-state NMR, X-ray diffraction, and pair distribution function analysis study. *J Am Chem Soc*. 2009;131(30):10525-10536.
50. Yamakawa N, Jiang M, Grey CP. Investigation of the conversion reaction mechanisms for binary copper (II) compounds by solid-state NMR spectroscopy and X-ray diffraction. *Chem Mater*. 2009;21(14):3162-3176.
51. Wang F, Robert R, Chernova NA, et al. Conversion reaction mechanisms in lithium ion batteries: study of the binary metal fluoride electrodes. *J American Chem Soc*. 2011;133(46):18828-18836.
52. Wang F, Yu HC, Chen MH, et al. Tracking lithium transport and electrochemical reactions in nanoparticles. *Nat Commun*. 2012;3(1):1-8.
53. Li L, Jacobs R, Gao P, et al. Origins of large voltage hysteresis in high-energy-density metal fluoride lithium-ion battery conversion electrodes. *J Am Chem Soc*. 2016;138(8):2838-2848.
54. Hua X, Robert R, Du LS, et al. Comprehensive study of the CuF_2 conversion reaction mechanism in a lithium ion battery. *J Phys Chem C*. 2014;118(28):15169-15184.
55. Hua X, Eggeman AS, Castillo-Martínez E, et al. Revisiting metal fluorides as lithium-ion battery cathodes. *Nat Mater*. 2021;20(6):841-850.
56. Fransson LM, Vaughey J, Benedek R, Edström K, Thomas JO, Thackeray M. Phase transitions in lithiated

Cu_2Sb anodes for lithium batteries: an in situ X-ray diffraction study. *Electrochem Commun*. 2001;3(7):317-323.

57. Chang D, Chen MH, Van der Ven A. Factors contributing to path hysteresis of displacement and conversion reactions in Li ion batteries. *Chem Mater*. 2015;27(22):7593-7600.
58. Bodenez V, Dupont L, Morcrette M, Surcin C, Murphy D, Tarascon JM. Copper extrusion/reinjection in Cu-based thiospinels by electrochemical and chemical routes. *Chem Mater*. 2006;18(18):4278-4287.
59. Lu Z, MacNeil D, Dahn J. Layered cathode materials $Li[Ni_xLi_{(1/3-2x/3)}Mn_{(2/3-x/3)}]O_2$ for lithium-ion batteries. *Electrochem Solid State Lett*. 2001;4(11):A191.
60. Thackeray MM, Kang SH, Johnson CS, Vaughey JT, Benedek R, Hackney S. Li_2MnO_3-stabilized $LiMO_2$ (M = Mn, Ni, Co) electrodes for lithium-ion batteries. *J Mater Chem*. 2007;17(30):3112-3125.
61. Rozier P, Tarascon JM. Li-rich layered oxide cathodes for next-generation Li-ion batteries: chances and challenges. *J Electrochem Soc*. 2015;162(14):A2490.
62. Zhang M, Kitchaev DA, Lebens-Higgins Z, et al. Pushing the limit of 3D transition metal-based layered oxides that use both cation and anion redox for energy storage. *Nat Rev Mater*. 2022.
63. Zuo W, Luo M, Liu X, et al. Li-rich cathodes for rechargeable Li-based batteries: reaction mechanisms and advanced characterization techniques. *Energy Environ Sci*. 2020;13(12):4450-4497.
64. Sathiya M, Rousse G, Ramesha K, et al. Reversible anionic redox chemistry in high-capacity layered-oxide electrodes. *Nat Mater*. 2013;12(9):827-835.
65. Koga H, Croguennec L, Ménétrier M, et al. Reversible oxygen participation to the redox processes revealed for $Li_{1.20}Mn_{0.54}Co_{0.13}Ni_{0.13}O_2$. *J Electrochem Soc*. 2013;160(6):A786.
66. Koga H, Croguennec L, Ménétrier M, et al. Operando X-ray absorption study of the redox processes involved upon cycling of the Li-rich layered oxide $Li_{1.20}Mn_{0.54}Co_{0.13}Ni_{0.13}O_2$ in Li ion batteries. *J Phys Chem C*. 2014;118(11):5700-5709.
67. Seo DH, Lee J, Urban A, Malik R, Kang S, Ceder G. The structural and chemical origin of the oxygen redox activity in layered and cation-disordered Li-excess cathode materials. *Nat Chem*. 2016;8(7):692-697.
68. Luo K, Roberts MR, Hao R, et al. Charge-compensation in 3D-transition-metal-oxide intercalation cathodes through the generation of localized electron holes on oxygen. *Nat Chem*. 2016;8(7):684-691.
69. Radin MD, Vinckeviciute J, Seshadri R, Van der Ven A. Manganese oxidation as the origin of the anomalous capacity of Mn-containing Li-excess cathode materials. *Nat Energy*. 2019;4(8):639-646.
70. House RA, Rees GJ, Pérez-Osorio MA, et al. First-cycle voltage hysteresis in Li-rich 3D cathodes associated with molecular O_2 trapped in the bulk. *Nat Energy*. 2020;5(10):777-785.
71. Vinckeviciute J, Kitchaev DA, Van der Ven A. A two-step oxidation Mechanism Controlled by Mn Migration explains the first-cycle activation behavior of Li_2MnO_3 -Based Li-Excess materials. *Chem Mater*. 2021;33(5):1625-1636.
72. Clément R, Lun Z, Ceder G. Cation-disordered rocksalt transition metal oxides and oxyfluorides for high energy lithium-ion cathodes. *Energy Environ Sci*. 2020;13(2):345-373.
73. Gent WE, Lim K, Liang Y, et al. Coupling between oxygen redox and cation migration explains unusual electrochemistry in lithium-rich layered oxides. *Nat Commun*. 2017;8(1):1-12.
74. Hong J, Gent WE, Xiao P, et al. Metal-oxygen decoordination stabilizes anion redox in Li-rich oxides. *Nat Mater*. 2019;18(3):256-265.
75. Taylor ZN, Perez AJ, Coca-Clemente JA, et al. Stabilization of O-O bonds by d0 Cations in $Li_{4+x}Ni_{1-x}WO_6$ ($0 x \leq 0.25$) rock salt oxides as the origin of large voltage hysteresis. *J Am Chem Soc*. 2019;141(18):7333-7346.
76. Zhao E, Zhang M, Wang X, et al. Local structure adaptability through multi cations for oxygen redox accommodation in Li-Rich layered oxides. *Energy Storage Mater*. 2020;24:384-393.
77. Natarajan AR, Thomas JC, Puchala B, Van der Ven A. Symmetry-adapted order parameters and free energies for solids undergoing order-disorder phase transitions. *Phys Rev B*. 2017;96(13):134204.
78. Van der Ven A, Thomas JC, Puchala B, Natarajan AR. First-principles statistical mechanics of multicomponent crystals. *Ann Rev Mater Res*. 2018;48:27-55.
79. Yin SC, Grondey H, Strobel P, Anne M, Nazar LF. Electrochemical property: structure relationships in monoclinic $Li_{3-y}V_2(PO_4)_3$. *J Am Chem Soc*. 2003;125(34):10402-10411.
80. Li B, Sougrati MT, Rousse G, et al. Correlating ligand-to-metal charge transfer with voltage hysteresis in a Li-rich rock-salt compound exhibiting anionic redox. *Nat Chem* 2021;13:1070-1080.
81. Batchelor RJ, Einstein FWB, Jones CHW, Fong R, Dahn JR. Crystal structure of Li_2FeS_2. *Phys Rev B*. 1988;37:3699-3702.
82. Hansen CJ, Zak JJ, Martinolich AJ, et al. Multielectron, cation and anion redox in lithium-rich iron sulfide cathodes. *J Am Chem Soc*. 2020;142:6737-6749.
83. See KA, Leskes M, Griffin JM, et al. Ab initio structure search and in situ ^7Li NMR studies of discharge products in the Li-S battery system. *J Am Chem Soc*. 2014;136(46):16368-16377.
84. Saha S, Assat G, Sougrati MT, et al. Exploring the bottlenecks of anionic redox in Li-rich layered sulfides. *Nat Energy*. 2019;4:977-987.
85. Nagarajan S, Hwang S, Balasubramanian M, Thangavel NK, Arava LMR. Mixed cationic and anionic redox in Ni and Co free chalcogen-based cathode chemistry for Li-ion batteries. *J Am Chem Soc*. 2021;143:15732-15744.
86. d'Entremont A, Pilon L. First-principles thermal modeling of electric double layer capacitors under constant-current cycling. *J Power Sources*. 2014;246:887-898.
87. Newman J, Thomas KE, Hafezi H, Wheeler DR. Modeling of lithium-ion batteries. *J Power Sources*. 2003;119-121:838-843.
88. Thomas KE, Newman J. Thermal modeling of porous insertion electrodes. *J Electrochem Soc*. 2003;150(2):A176.
89. d'Entremont AL, Pilon L. First-principles thermal modeling of hybrid pseudocapacitors under galvanostatic cycling. *J Power Sources*. 2016;335:172-188.
90. Thomas KE, Newman J. Heats of mixing and of entropy in porous insertion electrodes. *J Power Sources*. 2003;119-121:844-849.
91. Baek SW, Wyckoff KE, Butts DM, et al. Operando calorimetry informs the origin of rapid rate performance in microwave-prepared $TiNb_2O_7$ electrodes. *J Power Sources*. 2021;490:229537.

92. Baek SW, Preefer MB, Saber M, et al. Potentiometric entropy and operando calorimetric measurements reveal fast charging mechanisms in PNb_9O_{25}. *J Power Sources*. 2022;520:230776.
93. Van der Ven A, Ceder G, Asta M, Tepesch P. First-principles theory of ionic diffusion with nondilute carriers. *Phys Rev B*. 2001;64(18):184307.
94. Van der Ven A, Thomas JC, Xu Q, Swoboda B, Morgan D. Nondilute diffusion from first principles: Li diffusion in Li_xTiS_2. *Phys Rev B*. 2008;78(10):104306.
95. Bhattacharya J, Van der Ven A. First-principles study of competing mechanisms of nondilute Li diffusion in spinel Li_xTiS_2. *Phys Rev B*. 2011;83(14):144302.
96. Belak AA, Wang Y, Van der Ven A. Kinetics of anatase electrodes: the role of ordering, anisotropy, and shape memory effects. *Chem Mater*. 2012;24(15):2894-2898.
97. Kolli SK, Van der Ven A. Elucidating the factors that cause cation diffusion shutdown in spinel-based electrodes. *Chem Mater*. 2021;33(16):6421-6432.
98. Kaufman JL, Van der Ven A. Antiphase boundary migration as a diffusion mechanism in a P3 sodium layered oxide. *Phys Rev Mater*. 2021;5(5):055401.
99. Vinckevičiūtė J, Radin MD, Faenza NV, Amatucci GG, Van der Ven A. Fundamental insights about interlayer cation migration in Li-ion electrodes at high states of charge. *J Mater Chem A*. 2019;7(19):11996-12007.
100. Mortemard de Boisse B, Nishimura S-i, Watanabe E, et al. Highly reversible oxygen-redox chemistry at 4.1 V in $Na_{4/7-x}[\square_{1/7}Mn_{6/7}]O_2$ ($\square$: Mn Vacancy). *Adv Energy Mater*. 2018;8(20):1800409.
101. Song B, Tang M, Hu E, et al. Understanding the low-voltage hysteresis of anionic redox in $Na_2Mn_3O_7$. *Chem Mater*. 2019;31(10):3756-3765.
102. Kitchaev DA, Vinckeviciute J, Van der Ven A. Delocalized metal-oxygen π -redox is the origin of anomalous nonhysteretic capacity in Li-ion and Na-ion cathode materials. *J Am Chem Soc*. 2021;143(4):1908-1916.
103. Kwak WJ, Rosy, Sharon D, et al. Lithium-oxygen batteries and related systems: potential, status, and future. *Chem Rev*. 2020;120(14):6626-6683.
104. Liu T, Vivek JP, Zhao EW, Lei J, Garcia-Araez N, Grey CP. Current challenges and routes forward for nonaqueous lithium-air batteries. *Chem Rev*. 2020;120(14):6558-6625.
105. Pang Q, Liang X, Kwok CY, Nazar LF. Advances in lithium-sulfur batteries based on multifunctional cathodes and electrolytes. *Nat Energy*. 2016;1(9):1-11.

AUTHOR BIOGRAPHIES

Anton Van der Ven is professor of materials at the University of California Santa Barbara. His research seeks to unravel the links between the electronic structure of solids and their macroscopic properties using first-principles statistical mechanics. He studies a wide variety of materials classes for electrochemical energy storage and high-temperature structural applications. His group develops statistical mechanics methods and accompanying software tools to predict the properties of materials from first principles. He studied metallurgy and applied materials science at the Katholieke Universiteit Leuven and obtained a Ph.D. in Materials Science at the Massachusetts Institute of Technology.

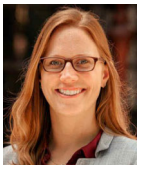

Prof. Kimberly A. See received her B.S. in chemistry from the Colorado School of Mines and her Ph.D. in chemistry from the University of California, Santa Barbara. After a postdoc at the University of Illinois at Urbana-Champaign, Kim began her independent career at Caltech as an Assistant Professor of Chemistry in the Division of Chemistry and Chemical Engineering. Her lab works on electrochemical interfaces and materials with a strong focus on next-generation battery chemistry.

Laurent Pilon is professor in the mechanical and aerospace engineering department at the University of California, Los Angeles (UCLA). His research group is engaged in a wide range of interdisciplinary research projects at the intersection of interfacial and transport phenomena, material science, and biology for the development of sustainable energy conversion, storage, and efficiency technologies. He and his collaborators have authored 6 book chapters and more than 180 archival journal publications, and 2 patents. Laurent Pilon is the recipient of several prestigious awards including the CAREER Award from the U.S. National Science Foundation (2005), the Bergles-Rohsenow Young Investigator Award in Heat Transfer (2008), and the Heat Transfer Memorial Award (2021) from the American Society of Mechanical Engineers. He received a bachelor's and a master's degree in applied physics from the Grenoble Institute of Technology, France and a Ph.D. in mechanical engineering from Purdue University.

How to cite this article: Van der Ven A, See KA, Pilon L. Hysteresis in electrochemical systems. *Battery Energy*. 2022;20210017. doi:10.1002/bte2.20210017